

A Droplet-Reactor System Capable of Automation for the Continuous and Scalable Production of Noble-Metal Nanocrystals

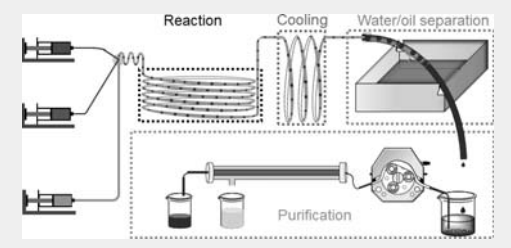
Guangda Niu, †,‡,§® Lei Zhang,† Aleksey Ruditskiy, ® Liduo Wang,§ and Younan Xia*,†,||,⊥®

[†]The Wallace H. Coulter Department of Biomedical Engineering, Georgia Institute of Technology and Emory University, Atlanta, Georgia 30332, United States

*Wuhan National Laboratory for Optoelectronics, Huazhong University of Science and Technology, Wuhan 430074, China

Supporting Information

ABSTRACT: Noble-metal nanocrystals with well-controlled shapes or morphologies are of great interest for a variety of applications. To utilize these nanomaterials in consumer products, one has to produce the colloidal nanocrystals in large quantities while maintaining good control over their physical parameters and properties. Droplet reactors have shown great potential for the continuous and scalable production of colloidal nanocrystals with controlled shapes. However, the efficiencies of most previously reported systems are still limited because of the complex post-treatment procedures. For example, the mixture of silicone oil and an aqueous suspension of solid



products has to be separated by leveraging their miscibility and difference in density, while the solid products often need to be purified and concentrated by centrifugation. Herein, we report the design and construction of a droplet-reactor system that include new features such as a homemade unit for the automatic separation of silicone oil from the aqueous phase as well as a cross-flow filtration unit for the effective purification and concentration of the nanocrystals. Using various types of Pd nanocrystals as examples, we have demonstrated the feasibility of using this system to automatically produce and collect samples with uniform sizes and well-controlled shapes.

KEYWORDS: Droplet reactor, automation, nanocrystals, separation, purification

notrolling the shape or morphology of noble-metal nanocrystals offers a viable approach to engineering their properties for enhanced performance in an array of applications such as catalysis, photonics, sensing, and imaging. 1-5 For example, it has been shown that the specific activities of Pd cubes and octahedra, enclosed by {100} and {111} facets, respectively, can differ by more than 10-fold when applied to catalyze the oxygen-reduction reaction (ORR). Despite these successful demonstrations, it is still challenging to directly transfer academic studies to industrial applications, primarily because of the inability to produce the colloidal nanocrystals at an industry-relevant scale while maintaining tight controls over their physicochemical properties. Taking the catalyst loaded in a three-way catalytic converter for a compact passenger vehicle as an example, 1-2 g of Pd, Rh, and Pt are typically needed, far beyond the production scale (typically, tens of milligrams) currently offered by a synthesis conducted in the laboratory setting.6

To address the aforementioned issue, a number of methods have been reported in literature for the scaling up of the production of colloidal nanocrystals. $^{7-10}$ In general, two different approaches can be used to scale up the production:

(i) increasing the reaction volume by switching to a larger batch reactor and (ii) decreasing the reaction volume by dividing the reaction solution into a continuous train of droplets. For the first approach, the quality of the product and the reproducibility are highly dependent on the type of reaction. A few attempts have been reported for the first approach, including the synthesis of penta-twinned Cu nanowires and Au nanorods. 11,12 The products were plagued by the poor quality and poor batchto-batch reproducibility. The reason can be attributed to the high sensitivity of both the nucleation and the growth processes to the experimental details, including the way a reagent is added into the reaction system, the management of heat for the involved endothermic and exothermic reactions as well as the chemical and heat transfer rates. Typically, none of these parameters or processes scale linearly with the reaction volume. Once the volume increases, the products are often marred by poor uniformity, with essentially no control over the shape and size. From the viewpoint of industrial applications, it is highly

Received: March 24, 2018 Revised: May 3, 2018 Published: May 7, 2018

[§]Key Lab of Organic Optoelectronics and Molecular Engineering of Ministry of Education, Department of Chemistry, Tsinghua University, Beijing 100084, China

 $^{^{\}parallel}$ School of Chemistry and Biochemistry and $^{\perp}$ School of Chemical and Biomolecular Engineering, Georgia Institute of Technology, Atlanta, Georgia 30332, United States

desired to obtain uniform products regardless of the reaction type. In the second approach, microfluidic and millifluidic devices have been developed to create a continuous flow of droplet reactors. ^{13,14} The droplet reactors provide many advantages, including the fast rates for thermal and mass transfer, the ability to rapidly screen reaction parameters, the low consumption of reagents during the optimization process, and the capability to operate multiple devices in parallel. ^{15–19} Because microfluidic devices are often troubled by a number of issues such as low throughput, irreversible reactor fouling during a synthesis, and complicated fabrication procedures, millifluidic devices have received increasing attentions for scaled-up production. ^{9,20}

Millifluidic devices for droplet reactors, also known as droplet-based millireactors, generate droplets with volumes on the scale of microliters to milliliters. These devices can be conveniently assembled from commercial polymeric tubes and silica capillaries. Several demonstrations have been reported for the shape-controlled synthesis of noble-metal nanocrystals using droplet-based millireactors, including Pd and Ag nanocubes, Au nanorods, and Ag triangular nanoprisms.^{21–24} In addition, the setup can also be integrated with techniques such as those based on X-ray scattering, photoluminescence, and UV-vis spectroscopy for in situ characterization. These techniques allow for the analysis of reaction kinetics and monitoring of the nucleation and growth processes, offering insightful guidance for engineering of the nanocrystals.²⁵ However, the current droplet-reactor system still lacks the capability for automated operation. The operator needs to manually collect and then separate the mixture of silicone oil and water as well as to purify the colloidal nanocrystals by centrifugation, electrophoresis, or chromatography. 21,28,29 These separation and purification methods only work for small-scale, batch-to-batch processing, significantly decreasing the overall production rate of a droplet-reactor system. Integrating the droplet-reactor system with online separation and purification units will allow for continuous and automatic operation, making the system well-suited for large-scale

Herein, we demonstrate the design and fabrication of a droplet-reactor system with the potential for automated operation by incorporating the capabilities of both water and oil separation and product purification into a millifluidic system. The device contains four major units (Figures 1 and S1), with each unit serving one particular function: (i) reaction, (ii) cooling, (iii) water and oil separation, and (iv) purification. The

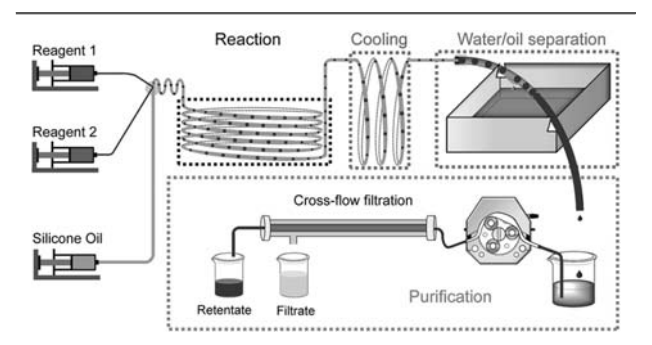


Figure 1. Schematic illustration of the droplet-reactor system with the potential for automation, which contains four units with the dedicated functions for reaction, cooling, water and oil separation, and purification, respectively.

reaction unit ensures the rapid mixing of reagents and provides sufficient reaction time for the controlled nucleation and growth of nanocrystals. The cooling unit rapidly quenches the reaction, producing nanocrystals with a particular composition and size. The water and oil separation unit is based on a polytetrafluoroethylene (PTFE) tube with a porous wall (see the Supporting Information for details). Silicone oil, acting as the carrier phase in the fluidic system, preferentially wets the PTFE tube and subsequently leaves the flow stream because of capillary action across the pores. Finally, the aqueous phase passes through the purification unit, where the residual chemicals (e.g., precursor, redundant, and capping agent) are removed via cross-flow filtration. Significantly, this online filtration system can also be used to separate nanowires from small nanoparticles. The synthesis of Pd nanocrystals with different sizes and shapes (cubes, octahedra, and nanowires) serves as a proof-of-concept example. We chose Pd as our initial focus because its nanocrystals have shown great promise as catalysts in a wide variety of applications such as Suzuki and Heck coupling reactions as well as hydrogen absorption and purification. 30

In the reaction unit, discrete droplets were generated using a simple fluidic device composed of two parallel silica capillaries inserted into a PTFE tube. As shown in Figure 1, the silica capillaries and the PTFE tube were connected to three syringes hosted in two syringe pumps to deliver the reaction and carrier phases separately at adjustable flow rates. The utilization of oil as a carrier phase can reduce the chance of fouling, and the setup can be reused multiple (>10) times. In comparison, if air is used as a carrier phase (as demonstrated later for the synthesis of nanowires), the reaction phase will be in direct contact with the tube and the products may stick to the surface. In this case, we have to wash the tube with dilute nitric acid to clean the inner surface of the tube. The rapid and effective mixing within each droplet was achieved through chaotic advection caused by the stretching and folding of the droplets. 15 The droplets then entered another segment of PTFE tube immersed in a temperature-controlled oil bath for the initiation and continuation of reaction. The residence time of the droplets in the reaction unit was adjusted by varying the length of the PTFE tube, the flow rates of the solutions, or both. In a typical experiment, when a PTFE tube with a length of 7.5 m and an inner diameter (I.D.) of 1.58 mm was used, a residence time of 20 min was achieved by setting the flow rates for the silicone oil and aqueous reaction solution to 0.5 and 0.1 mL/min, respectively. Our previous work has demonstrated that the quality of the as-produced nanocrystals could be preserved, with the I.D. of the PTFE tube varying from 0.5 to 5.8 mm. However, for smaller diameters, the tube is susceptible to fouling and clogging and thereby may hinder the long-term operation. 33,34 The growth of nanocrystals was then terminated by driving the droplets through a segment of PTFE tube immersed in an ice-water bath. It should be noted that the quantity of the products could be further scaled up by increasing the operation time, as was demonstrated in our previous work.³⁴

After flowing through the reaction and cooling units, the aqueous droplets and the silicone oil entered the water and oil separation unit. The unit consisted of an oil-collection box and a 33 cm long PTFE tube with an I.D. of 5.8 mm with a surface partially covered by pinholes (see the details in the Supporting Information), as shown in Figure 1. The pinholes were fabricated by punching with a 30 G needle (with an outer

diameter, or O.D., of 311 μ m) through the wall of the PTFE tube. The pinholes provided pathways for the outflow of oil, as illustrated in Figure 2a,b. Due to the hydrophobicity of the

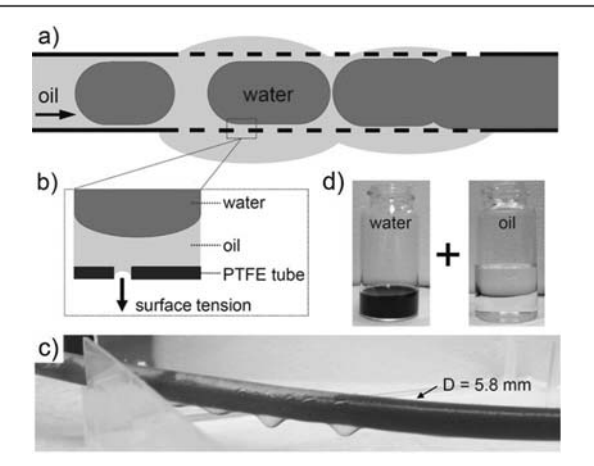


Figure 2. Illustrations of the water and oil separation unit. (a) Schematic of the process for water and oil separation: the silicone oil permeates through the porous PTFE tube, while the water phase remains in the channel. (b) Schematic illustration of the separation mechanism, with surface tension serving as the driving force. (c) A snapshot of the device during online water and oil separation. (d) Photographs of the separated phases collected after running for 10 min with the flow rates for water and oil phases set to 0.4 and 1.0 mL/min, respectively.

PTFE tube, the silicone oil preferentially wetted the tube and formed a convex meniscus in the pinhole, whereas water formed a flat surface in the pinhole (Figure S2). The capillary action caused by the convex meniscus provided the necessary driving force to push the silicone oil out of the PTFE tube (Figure 2b).

According to the Young–Laplace equation of capillary action, we could calculate the pressure drop across the interface between silicone oil and air in the pinhole:³⁵

$$\Delta p = \frac{2\gamma}{R} \tag{1}$$

$$R = \frac{a}{\cos \theta} \tag{2}$$

where Δp is the pressure drop across the surface, γ is the surface tension of silicone oil (20.1 mN/m), R is the radius of the spherical meniscus formed at the interface, θ is the contact angle between the silicone oil and the PTFE tube, and a is the radius of a pinhole (311 μ m). The contact angle, θ , between silicone oil and PTFE tube was measured to be 27°, as shown in Figure S2a. Therefore, the pressure drop across the interface of the convex meniscus in the pinhole could reach 115 Pa. Consequently, a column of silicone oil with a height of 1.2 cm could form inside the pinhole according to the following hydrostatic equilibrium equation:

$$\Delta p = \rho g h \tag{3}$$

where ρ is the density of silicone oil (0.934 g/mL), g is the gravitational acceleration (9.8 m/s²), and h is the height of silicone oil. The wall thickness of the PTFE tube used in the water and oil separation device was only 0.275 mm, far less than 1.2 cm. Therefore, the pressure drop was sufficient to push the silicone oil out of the PTFE tube through the pinholes. The

water phase remained in the tube because the aqueous solution could not wet the hydrophobic PTFE tube (Figure S2b). The movement of both the oil and the aqueous phases could be clearly seen in the video in the Supporting Information. The silicone oil was rapidly removed from the tube after the liquid had traveled a few centimeters through the porous segment (Figure 2c). To confirm that the purification unit had successfully separated the aqueous phase from silicone oil, we collected the aqueous and oil phases separately after 10 min of operation. As shown in Figure 2d, the aqueous and oil phases in the separate bottles verify the effective and complete separation of the two phases. It should be pointed out that a similar concept based on a porous membrane has been applied to the separation of immiscible liquids.^{36–38} While membrane-based separation can also be applied to the synthesis of nanocrystals, it needs additional steps to be integrated with a fluidic system for online separation. The requirement for an accurate control over the pressure makes the membrane-based separation less convenient than the technique based on a porous PTFE tube. 39,40

In the final step, we integrated a cross-flow filtration unit into the system as a replacement for the conventional centrifugation process. Cross-flow filtration is a mature technique for the size separation and purification of proteins. Here we demonstrated the incorporation of cross-flow filtration as an online component in a droplet-reactor system for the separation and purification of nanocrystals. Figure 3 shows a schematic

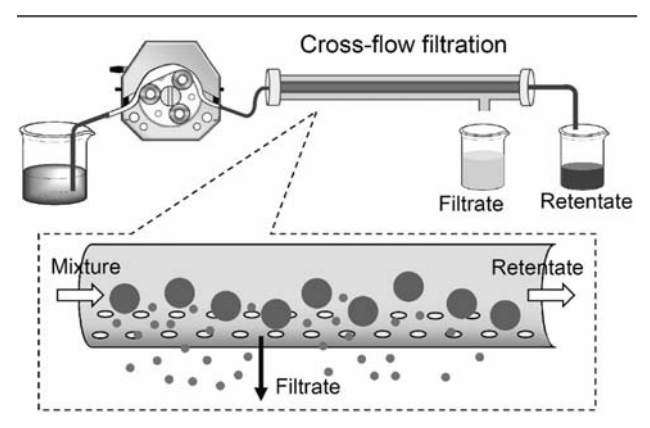


Figure 3. Schematic of the setup for cross-flow filtration. The solution was driven by a peristaltic pump. As restricted by the size of the pores in the hollow-fiber membrane, the solvent, unreacted precursor, redundant, capping agent, and small nanoparticles can penetrate through the pores and leave the hollow fiber, while the large nanoparticles remain inside the flow channel.

illustration of the cross-flow filtration setup used in this work, wherein the filter was composed of a hollow-fiber membrane. During cross-flow filtration, the mixture solution flows along a direction perpendicular to the filtration direction. In this work, a peristaltic pump was employed to continuously drive the aqueous phase collected from the water and oil separation unit into a 50 kDa filter, with an average pore size of approximately 6–8 nm in diameter. The filter is rated by the nominal molecular weight cutoff (MWCO), and a 50 kDa filter is supposed to retain 90% of a globular protein with a molecular mass of >50 kDa. The solvent, unreacted precursor and redundant, and capping agent should all be able to permeate through the filter, while Pd nanoparticles would be trapped in the flow channel (considering their larger sizes relative to the

pore size). The outlet of the filter was connected to a syringe needle to help increase the liquid pressure inside the filter (Figure S1). The increased pressure could enhance the permeation rate. With this approach, 10 mL of a solution could be concentrated to 0.45 mL after a single run, with the pumping rate of the peristaltic pump fixed at 10 mL/min. Typically, the concentrated solution needed to be purified three more times to ensure complete purification of the products by diluting the concentrated suspension with 10 mL of water and repeating the filtration process.

As shown in Figure 4, Pd nanocrystals with controlled sizes and shapes could be readily obtained using the automated

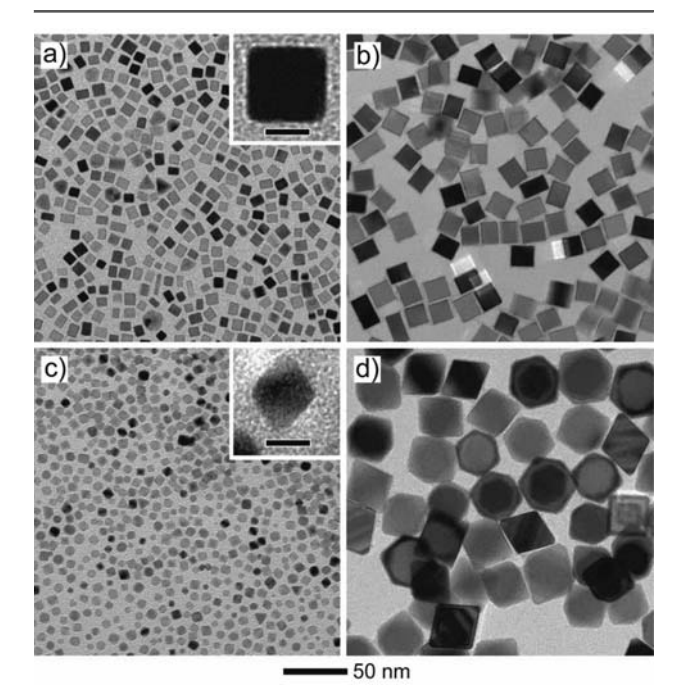


Figure 4. TEM images of the as-obtained Pd nanocrystals with different shapes: (a) 8 nm Pd cubes, (b) 16 nm Pd cubes, (c) 6 nm Pd octahedra, and (d) 35 nm Pd octahedra grown from the 16 nm Pd cubic seeds. The scale bars in the insets correspond to 5 nm.

fluidic device by choosing different combinations of capping agent, reductant, and reaction temperature according to the protocols previously reported for batch reactors. The detailed experimental conditions can be found in the Supporting Information. For Pd nanocubes covered by {100} facets, they were produced by employing Na₂PdCl₄ as a salt precursor, Lascorbic acid as a reducing agent, KBr as a capping agent, and poly(vinylpyrrolidone) (PVP) as a colloidal stabilizer. According to the previous reports, the edge length of the Pd nanocubes could be tuned by adjusting the ratio of KBr to Na₂PdCl₄.^{21,43} Specifically, Pd nanocubes of 8 nm (Figure 4a) and 16 nm (Figure 4b) in edge length were successfully synthesized in the device using 300 and 600 mg KBr, respectively. The edge lengths were calculated by averaging the measurements on 100 particles (Figure S3). Furthermore, we synthesized Pd octahedra by modifying existing protocols for batch synthesis. 44,45 Figure 4c shows TEM images of 6 nm Pd octahedra prepared using Na₂PdCl₄ as a salt precursor, citric acid as a capping agent, and PVP as a colloidal stabilizer in a mixture of water and ethanol. The size and shape uniformity of the resultant products were similar to those prepared in batch

reactors. He was also demonstrated the use of the droplet reactors for seed-mediated growth to further diversify the size of the Pd octahedra by introducing PVP as a stabilizer, formaldehyde (HCHO) as a mild reducing agent, and Na_2PdCl_4 as a salt precursor into a suspension of Pd nanocubes at 60 °C. During this process, the 16 nm Pd cubes were directed to evolve into Pd octahedra with an edge length of 35 nm (Figure 4d).

The TEM samples shown in Figure 4 were prepared by directly drop-casting the reaction products obtained through this device onto copper grids without any other treatments. The clear images suggest that the residual PVP in the solution, which did not attach to the nanocrystals, had been washed away. The filter eluent was further freeze-dried to generate a flaxen powder. Fourier transform infrared spectroscopy (FTIR) of the powder (Figure S4) verified the presence of PVP in the eluent. Similarly, we believe that the unreacted precursor and redundant as well as the capping agent were also effectively washed away through the cross-flow filtration because of their good solubility in water.

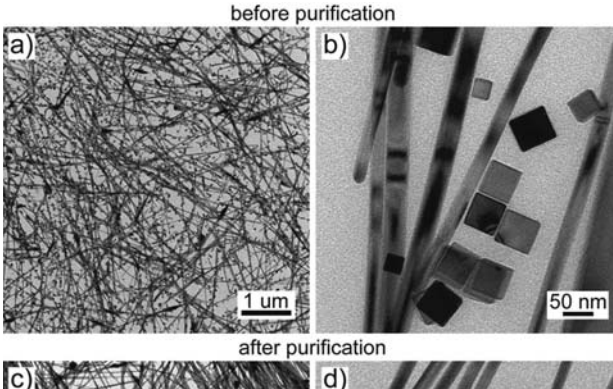
Moreover, the cross-flow filtration facilitated greater collection efficiency compared to the conventional centrifugation method. To demonstrate this, we measured the Pd contents of the samples of 8 nm Pd nanocubes collected by centrifugation and cross-flow filtration, respectively, using inductively coupled plasma mass spectrometry (ICP-MS). Table 1 compares the Pd contents and collection efficiencies

Table 1. Comparison of the Two Methods for the Purification of 8 nm Pd Cubes

	Pd concentration (mg/mL)	collection efficiency (%)
centrifugation	1.455	77.6
cross-flow filtration	1.637	87.4

for these two approaches. The collection efficiency was calculated as the ratio of the collected Pd to the Pd present in the original precursor solution. The cross-flow filtration method showed a greater collection efficiency of 87.4% in comparison to centrifugation, which had a collection efficiency of 77.6%. During centrifugation, some nanoparticles can remain in the supernatant because the applied centrifugal force may not be sufficiently strong to collect all the nanocrystals. In cross-flow filtration, the particles should not be able to escape from the filter based on the size difference between the nanoparticles and pores.

The automated fluidic device was also applied to the synthesis of anisotropic nanocrystals such as penta-twinned Pd nanowires. We followed our previously reported protocol, with the use of air as a carrier phase, Na₂PdCl₄ as a metal precursor, L-ascorbic acid as a reductant, NaI as a capping agent, diethylene glycol as a solvent, and HCl as an additive to adjust the reaction kinetics. 46 Due to the absence of oil, there is no need to include the separation unit. The as-obtained solid products contained a mixture of Pd nanowires and nanocubes, as shown in Figure 5a,b. The lengths of the Pd nanowires varied from 0.5 to 2 μ m, while the average diameter was 12.9 \pm 2.1 nm, as calculated from 100 nanowires (Figure S5a). The nanocubes had an average edge lengths of 24.5 ± 3.4 nm (Figure S5b). The cubic component must be removed before the nanowires can be used in applications such as electronics and display because the impurities tend to interfere with electron transfer in a network of nanowires.⁴⁷ As reported in



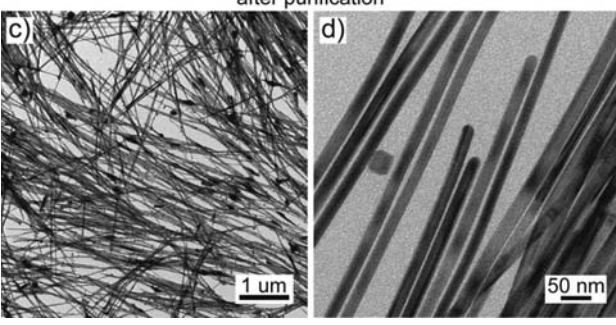


Figure 5. TEM images of Pd nanowires before and after purification by cross-flow filtration. (a,b) The as-obtained mixture of Pd nanowires and nanocubes and (c,d) the nanowire concentrate after purification by cross-flow filtration.

the literature, such a mixture can be separated using a technique such as gradient centrifugation. ⁴⁸ In our case, we were able to purify the nanowires using a cross-flow filtration tube with a pore size of $0.2~\mu m$. In such a setup, the Pd nanocubes would flow through the hollow membrane and get out of the filter, while the nanowires were prevented from passing through the membrane due to their much-greater dimensions along the axial direction. Consequently, the Pd nanocubes present in the as-obtained product (Figure 5a,b) was effectively removed through cross-flow filtration, generating a pure sample of Pd nanowires (Figure 5c,d).

In summary, we have demonstrated a droplet-reactor system that can be automated for the production of noble-metal nanocrystals with uniform sizes and well-controlled shapes. The system contains a water and oil separation unit for removing the silicone oil through the pores in the wall of a PTFE tube through capillary action, as driven by favorable wetting. We have also demonstrated that cross-flow filtration could be integrated with the droplet-reactor system to give an online purification option for the selective removal of unused precursor, redundant, capping agent, and stabilizer, as well as byproducts with undesired sizes or shapes, from the as-obtained product of a synthesis. Although we have mainly focused on Pd nanocrystals, the approach is expected to be extendible to other systems. Once automated with online separation and purification capabilities, this system provides a simple and robust route to the continuous and scalable production of noble-metal nanocrystals for industrial applications.

ASSOCIATED CONTENT

Supporting Information

The Supporting Information is available free of charge on the ACS Publications website at DOI: 10.1021/acs.nanolett.8b01200.

Fabrication procedures and experimental details. Figures showing photographs of the system, FTIR spectra of the eluent, and size distributions of the as-obtained nanocrystals. (PDF)

A video showing the movement of both the oil and the aqueous phases. (AVI)

AUTHOR INFORMATION

Corresponding Author

*E-mail: younan.xia@bme.gatech.edu.

ORCID ®

Guangda Niu: 0000-0002-9285-4147 Aleksey Ruditskiy: 0000-0002-1146-827X Younan Xia: 0000-0003-2431-7048

Notes

The authors declare no competing financial interest.

ACKNOWLEDGMENTS

This work was supported in part by the National Science Foundation (grant no. CMMI-1634687) and startup funds from the Georgia Institute of Technology. G.N. is thankful for support from the China Scholarship Council.

■ REFERENCES

- (1) Burda, C.; Chen, X.; Narayanan, R.; El-Sayed, M. A. Chem. Rev. 2005, 105, 1025-1102.
- (2) Xia, Y.; Xiong, Y.; Lim, B.; Skrabalak, S. E. Angew. Chem., Int. Ed. **2009**, 48, 60–103.
- (3) Zhou, K.; Li, Y. Angew. Chem., Int. Ed. 2012, 51, 602-613.
- (4) Camden, J. P.; Dieringer, J. A.; Zhao, J.; Van Duyne, R. P. Acc. Chem. Res. **2008**, 41, 1653–1661.
- (5) Rosi, N. L.; Mirkin, C. A. Chem. Rev. 2005, 105, 1547-1562.
- (6) Tollefson, J. Nature 2007, 450, 334-335.
- (7) Liu, B.; Chen, H. M.; Liu, C.; Andrews, S. C.; Hahn, C.; Yang, P. J. Am. Chem. Soc. **2013**, 135, 9995–9998.
- (8) Martinez-Rodriguez, R. A.; Vidal-Iglesias, F. J.; Solla-Gullon, J.; Cabrera, C. R.; Feliu, J. M. J. Am. Chem. Soc. 2014, 136, 1280–1283.
- (9) Lohse, S. E.; Eller, J. R.; Sivapalan, S. T.; Plews, M. R.; Murphy, C. J. ACS Nano 2013, 7, 4135–4150.
- (10) Wu, F.; Zhang, D.; Peng, M.; Yu, Z.; Wang, X.; Guo, G.; Sun, Y. Angew. Chem., Int. Ed. **2016**, 55, 4952–4956.
- (11) Rathmell, A. R.; Bergin, S. M.; Hua, Y. L.; Li, Z. Y.; Wiley, B. J. Adv. Mater. 2010, 22, 3558-3563.
- (12) Jana, N. R. Small 2005, 1, 875-882.
- (13) Shestopalov, I.; Tice, J. D.; Ismagilov, R. F. Lab Chip 2004, 4, 316-321.
- (14) Chan, E. M.; Alivisatos, A. P.; Mathies, R. A. J. Am. Chem. Soc. **2005**, 127, 13854–13861.
- (15) Song, H.; Tice, J. D.; Ismagilov, R. F. Angew. Chem. 2003, 115, 792-796.
- (16) Zhang, M.; Wei, L.; Chen, H.; Du, Z.; Binks, B. P.; Yang, H. J. Am. Chem. Soc. 2016, 138, 10173–10183.
- (17) Niu, G.; Zhou, M.; Yang, X.; Park, J.; Lu, N.; Wang, J.; Kim, M. J.; Wang, L.; Xia, Y. Nano Lett. **2016**, 16, 3850–3857.
- (18) Moore, J. S.; Jensen, K. F. Angew. Chem. 2014, 126, 480-483.
- (19) Yashina, A.; Lignos, I.; Stavrakis, S.; Choo, J.; deMello, A. J. J. Mater. Chem. C 2016, 4, 6401–6408.
- (20) Nightingale, A. M.; Bannock, J. H.; Krishnadasan, S. H.; O'Mahony, F. T. F.; Haque, S. A.; Sloan, J.; Drury, C.; Mcintyre, R.; deMello, J. C. *J. Mater. Chem. A* **2013**, *1*, 4067–4076.
- (21) Kim, Y. H.; Zhang, L.; Yu, T.; Jin, M.; Qin, D.; Xia, Y. Small **2013**, 9, 3462–3467.
- (22) Zhang, L.; Wang, Y.; Tong, L.; Xia, Y. Langmuir 2013, 29, 15719–15725.

(23) Nightingale, A. M.; Krishnadasan, S. H.; Berhanu, D.; Niu, X.; Drury, C.; Mcintyre, R.; Valsami-Jones, E.; deMello, J. C. *Lab Chip* **2011**, *11*, 1221–1227.

- (24) Knauer, A.; Csáki, A.; Möller, F.; Hühn, C.; Fritzsche, W.; Köhler, J. M. J. Phys. Chem. C 2012, 116, 9251–9258.
- (25) Peng, S.; Okasinski, J. S.; Almer, J. D.; Ren, Y.; Wang, L.; Yang, W.; Sun, Y. *J. Phys. Chem. C* **2012**, *116*, 11842–11847.
- (26) Liu, Q.; Gao, M.-R.; Liu, Y.; Okasinski, J. S.; Ren, Y.; Sun, Y. Nano Lett. 2016, 16, 715–720.
- (27) Lignos, I.; Stavrakis, S.; Nedelcu, G.; Protesescu, L.; deMello, A. J.; Kovalenko, M. V. Nano Lett. 2016, 16, 1869–1877.
- (28) Templeton, A. C.; Cliffel, D. E.; Murray, R. W. J. Am. Chem. Soc. 1999, 121, 7081–7089.
- (29) Al-Somali, A. M.; Krueger, K. M.; Falkner, J. C.; Colvin, V. L. Anal. Chem. 2004, 76, 5903-5910.
- (30) Reetz, M. T.; deVries, J. G. Chem. Commun. 2004, 21, 1559-1563.
- (31) Sun, Y.; Tao, Z.; Chen, J.; Herricks, T.; Xia, Y. J. Am. Chem. Soc. **2004**, 126, 5940–5941.
- (32) Kim, S. W.; Kim, M.; Lee, W. Y.; Hyeon, T. J. Am. Chem. Soc. **2002**, 124, 7642–7643.
- (33) Zhang, L.; Xia, Y. Adv. Mater. 2014, 26, 2600-2606.
- (34) Zhang, L.; Niu, G.; Lu, N.; Wang, J.; Tong, L.; Wang, L.; Kim, M. J.; Xia, Y. Nano Lett. 2014, 14, 6626–6631.
- (35) De Gennes, P. G.; Brochard-Wyart, F.; Quéré, D. Capillarity and wetting phenomena: drops, bubbles, pearls, waves; Springer: Dordrecht, The Netherlands, 2004; p 6.
- (36) Bannock, J. H.; Phillips, T. W.; Nightingale, A. M.; deMello, J. C. Anal. Methods 2013, 5, 4991–4998.
- (37) Phillips, T. W.; Bannock, J. H.; deMello, J. C. Lab Chip 2015, 15, 2960–2967.
- (38) Crick, C. R.; Ozkan, F. T.; Parkin, I. P. Sci. Technol. Adv. Mater. 2015, 16, 055006.
- (39) Adamo, A.; Heider, P. L.; Weeranoppanant, N.; Jensen, K. F. Ind. Eng. Chem. Res. 2013, 52, 10802-10808.
- (40) Shen, Y.; Weeranoppanant, N.; Xie, L.; Chen, Y.; Lusardi, M. R.; Imbrogno, J.; Bawendi, M. G.; Jensen, K. F. *Nanoscale* **2017**, *9*, 7703–7707.
- (41) Sweeney, S. F.; Woehrle, G. H.; Hutchison, J. E. J. Am. Chem. Soc. 2006, 128, 3190–3197.
- (42) Trefry, J. C.; Monahan, J. L.; Weaver, K. M.; Meyerhoefer, A. J.; Markopolous, M. M.; Arnold, Z. S.; Wooley, D. P.; Pavel, I. E. *J. Am. Chem. Soc.* **2010**, *132*, 10970–10972.
- (43) Jin, M.; Liu, H.; Zhang, H.; Xie, Z.; Liu, J.; Xia, Y. Nano Res. **2011**, 4, 83–91.
- (44) Shao, M.; Yu, T.; Odell, J. H.; Jin, M.; Xia, Y. Chem. Commun. **2011**, 47, 6566–6568.
- (45) Jin, M.; Zhang, H.; Xie, Z.; Xia, Y. Energy Environ. Sci. 2012, 5, 6352–6457.
- (46) Peng, H.-C.; Li, Z.; Aldahondo, G.; Huang, H.; Xia, Y. J. Phys. Chem. C 2016, 120, 11754–11761.
- (47) Pradel, K. C.; Sohn, K.; Huang, J. Angew. Chem., Int. Ed. 2011, 50, 3412–3416.
- (48) Sun, X.; Tabakman, S. M.; Seo, W. S.; Zhang, L.; Zhang, G.; Sherlock, S.; Bai, L.; Dai, H. Angew. Chem., Int. Ed. 2009, 48, 939–942.